doi: 10.31674/book.2024ecc.004

Diversity of Zinc Oxide-Nanoconjugate: Photophysical and Photochemical Aspect

Piyali Mitra

Department of Chemistry (UG+PG), Trivenidevi Bhalotia College, Paschim Bardhaman, West Bengal, India

Corresponding Author's Email: mitra.piyali.2009@gmail.com

Abstract

Photophysical and photochemical studies of anticancer drug-functionalized nanoparticles are of enormous significance. Now adays, these nanoconjugates have greater application in the field of novel photo-based nanodevices for photocatalysis and drug delivery. Moreover, nanoconjugates are anticipated to be excellent revenue of assimilating attractive features of molecular as well as bulk regimes. Nanostructured materials produce the electronic excited states, or excitons, during light-matter interactions. It is interesting to be acquainted with diverse kinds of electrons. Furthermore, gaining knowledge about a diverse range of materials is energizing, as it allows us to understand the formation of electronically excited states and progress into femtosecond and nanosecond time domains. The mechanism of solar energy conversion, which is a solely photo-initiated process using ultrafast lasers, as well as finding out about new photonic and biphotonic applications, are also important areas of now days' research. Researchers use hundreds of light-absorbing molecules, known as chromophores, to harvest sunlight. Chromophores also play an important role in directing the excitation energy to nature's solar cells- proteins, which are called reaction centers.

Keywords: *Biophotonic; Excitons; Graphene; Photodynamic Therapy; Quantum Dots (Qds); Reactive Oxygen Species (ROS); Solar Energy; Ultrafast Spectroscopy*

Introduction

Metal oxide nanomaterials have received a lot of attention due to their current and potential commercial importance. ZnO, in particular, is an excellent candidate for applications in photocatalyst, photodetector, and biomedicine. To date, a number of strategies have been employed to improve the photocatalytic operation of ZnO, primarily to reduce the recombination of photogenerated electrons and holes. In general, ZnO nanoparticles have gotten a lot of attention because they are very sensitive to light, strong at high temperatures, cheap, safe, and compatible with living things. This makes them a good choice for studying photocatalytic action as well as their important roles in biology (Yuan, Hein & Misra, 2010). First, Yuan, Hein and Misra (2010) used ZnO QDs

(quantum dots) attached to biodegradable molecules, like chitosan, to deliver drugs specifically to tumors. Specifically, they encrusted ZnO QDs with folate-conjugated chitosan via electrostatic interaction. The conjugation serves the purpose of loading the ZnO QDs with doxorubicin (DOX), a widely used chemotherapy drug, to achieve a 75% efficiency in action. Furthermore, Liu *et al*. (2016) reported a pH-responsive drug delivery system based on ZnO NP loaded with the anticancer drug, DOX. Moreover, numerous literature reports have demonstrated the enhanced photocatalytic and antibacterial activity of noble metal/zinc oxide hybrid nanostructures, indicating their immense potential for use in water purification and various pathogenic applications (He *et al*., 2014; Hu *et al*., 2016; Kumar *et al*., 2014; Mao *et al.,* 2017). ZnO nanostructured substances don't dissolve well in physiological media, but they can dissolve as nontoxic ions in acidic media, like the late endosome and lysozome of tumor cells (Wang *et al*., 2014; Xiong, 2013; Cho *et al*., 2011), and they can also dissolve in basic media (Abdelmonem *et al*., 2015). Because of their excellent properties, ZnO NPs have become very important as multifunctional nanocarriers that make the release process easier (Zhou *et al*., 2006). Also, ZnO nanoparticles can effectively carry drugs in photodynamic therapies (PDT) by stopping a lot of drug buildup at the desired site (Zhang *et al.,* 2013).

It is made up of 9AA-HCl (9-aminoacridine hydrochloride hydrate), which is an organic molecule whose spectral properties are very sensitive to its surroundings. Moreover, 9AA-HCl exists in three different structures depending on the pH of the medium (Scheme 1) (Mitra *et al*., 2014). In addition, it acts as one of the important drugs for antibacterial, mutagenic, and antitumor effects (Zhu *et al*., 1994). One intriguing biological use of 9AA-HCl is as an intercalant agent, which means it can mix with DNA (Rehn and Pindur, 1996; Wynn *et al*., 2017; Graham *et al*., 2011; Ceron-Carrasco *et al*., 2017). Latterini and Tarpani (2011), apply the fluorescent drug for membrane imaging after doping with silica nanoparticles. Furthermore, conjugation with gold nanoparticles also enhances the antibacterial activity of 9AA-HCl (Mitra, Chakraborty & Basu, 2014). The literature also reports that the PP-ZnO nanohybrid demonstrates enhanced photodynamic action to inhibit E. coli growth (Sardar *et al*., 2015). During the interaction between PDT drugs and semiconductor nanoparticles, the development of reactive oxygen species (ROS) is the foremost factor. ROS oxidizes the organic compound; therefore, ROS generation may also influence the photocatalytic action of semiconductors (Zhou *et al*., 2011). The quick recombination of photogenerating electron-hole pairs, faster than surface redox reactions, reduces the quantum efficiency of photocatalysis of the semiconductor (Hoffmann *et al*., 1995). Therefore, Luo *et al*. (2012) conjugate the semiconductor nanoparticles with other molecules or materials to enhance charge separation and prevent the recombination of the respective electron and hole pairs.

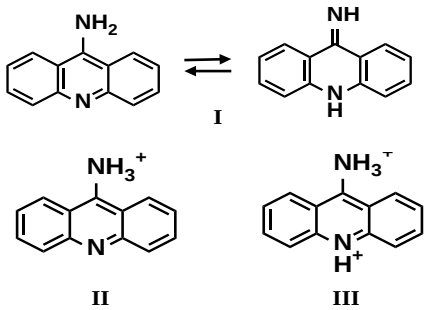

Scheme 1: The pH-responsive drug 9AA-HCl comes in various forms:(I) neutral; (II) protonated; (III) doubly protonated

Methodology and synthesis of ZnO nanoparticles

A transmission electron microscope (JEOL-TEM 2100 with an operating voltage of 200 kV) was used for the purpose of taking TEM images. To find out the crystal structures of the samples, an X-ray diffractometer with the model number Seifert 3000P and CuKa radiation (λ = 1.54178É) was used. The XPS data was obtained using Omicron nanotechnology. Zetasizer Nanosystem, Malvern Instruments Ltd., was used to calculate the DLS and zeta potential. A UV-vis spectrophotometer (SHIMADZU) was employed to measure the optical absorption spectra at room temperature. The fluoromax spectrophotometer of HORIBA JOBIN YVON was used to record the respective emission spectra (photoluminescence). Moreover, TCSPC, i.e., time-correlated single-photon counting measurement, was performed using picosecond NANO-LED. Using a previously reported method, ZnO NPs were synthesized (Barman *et al*., 2017).

Results and Discussion

Transmission electron microscope *i.e.,* TEM, Fourier transform infrared spectroscopy *i.e.,* FTIR and Raman spectroscopy are being used to establish the formation of nanoparticles as well as nano conjugation.

Zinc oxide nanoparticles

Figure 1A. depicts the TEM image with the particle size distribution, which depicts a monodispersed character with a particle size of ~6 ± 0.5 nm. Figure 1B. illustrates the XRD model for NPs. As expected, the XRD data shows that the nanoparticles are exactly the same as ZnO in its pure form, with a wurtzite nature configuration and a hexagonal crystal phase. Additionally, the XPS spectrum having two structural peaks implies ZnO of pure phase (at 1020.5 eV, it signifies $Zn2p_{3/2}$, and at 1043.9 eV, it signifies $Zn2p_{1/2}$). The UV-Vis spectrum shows evidence of pure ZnO NP, which corresponds to a band peak at 334 nm as depicted in Figure 1C. This UV data indicates that there is a restricted

size distribution of NP. Moreover, ZnO NP at 557 nm exhibits a strong yellow emission (Figure 1C), which is primarily caused by an oxygen vacancy defect in ZnO. Figure 1D. displays the TCSPC data for ZnO NP, which depicts defect emission with bi-exponential decay kinetics**.**

Furthermore, it is calculated from the obtained data that the lifetimes of the faster component are 7.69 ns (55%), and the slower component is 42.99 ns (45%), with an average lifetime of ~23.74 ns. While the emissions in the visible region are a tranquil topic of argument and quite a lot of explanations have been projected, the photoluminescence lifetime determines the concentration of defects. This type of emission occurs owing to the recombination of a trivial trapped electron in the midst of a profoundly trapped hole. In this current scenario, 43.0 ns, which signifies the longer lifetime component, happens owing to such recombination in the course of surface defects responsible for O^{2-}/O^{-}. The faster lifetime factor of ~7.7 ns originates from the band gap correlated with exciton recombination.

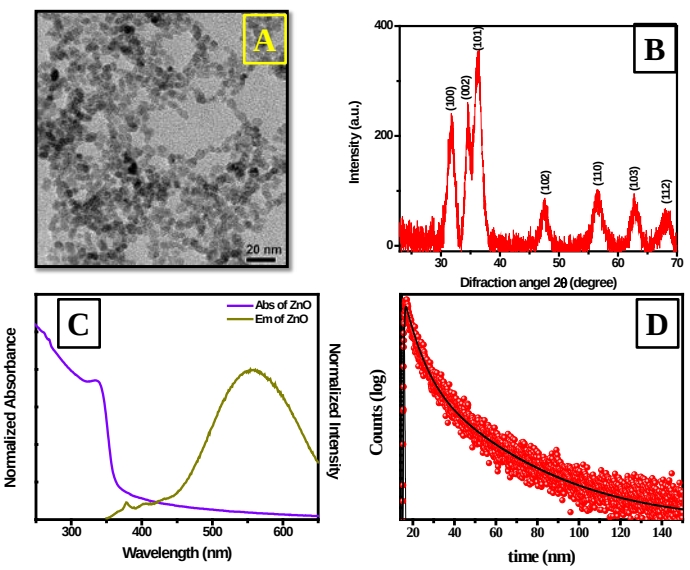

Figure 1: Zinc oxide nanoparticles (A) TEM image; (B) XRD pattern; (C) absorption and emission spectra; and (D) time-resolved decay curve *(Source: Baarman et al., 2017)*

Zinc oxide nanoconjugates

Small and consistently sized particles are of significant necessity to modulate physico-chemical properties, together with luminescence and drug-loading ability. The TEM image of nanohybrid is depicted in Figure 2. The consistencies of nearly spherical nanocrystals are confirmed.

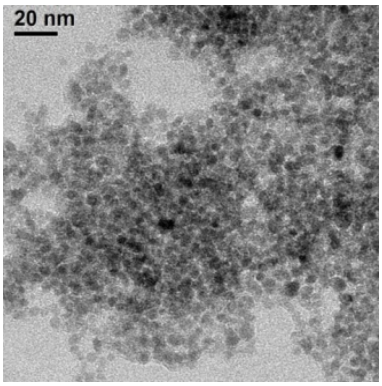

Figure 2 : ZnO-9AA-HCl nanoconjugate: Transmission electron micrograph.
(Source : Mitra et al., 2018)

Fourier transform infrared (FTIR) technique was used for studying the conjugation among the drug and the NP. The binding is a very essential factor for biological application. The FTIR spectra (Figure 3) having distinctive peak at 3337 $cm^{-1}$of drug molecule corresponds toward the amine group (-NH_2) stretching frequency (Mitra *et al*., 2014). However, subsequent to conjugation along with the NP, the stretching frequency which is responsible for of the -NH_2 moiety of the bare drug molecule is altered as well as broadened. The IR data signifies the fact that the covalent bonding is responsible for stretching frequency shifting. The covalent bond is formed between the -NH_2 (amine group) of the drug molecule and ZnO NP (Sardar *et al*., 2015). Moreover, owing to the conjugation, the surface hydroxyl groups of the ZnO (Liu *et al*., 2014, Tu *et al*., 2011) are affected (3370-3400 cm^{-1} and 1630-1635 cm^{-1}). This diminution in the intensity as well as shifting of the band position signifies the presence of hydrogen bonding interaction between nanoprticle and drug molecule (Das *et al*., 2017, Zhang *et al*. 2015).

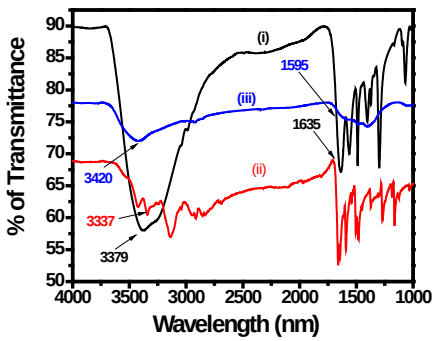

Figure 3: FTIR spectra of (i) NP, (ii) Drug molecule, and (iii) conjugate
(Source: Mitra et al., 2018)

The changes in the vibrational mode of ZnO NP after conjugation were investigated using a Raman spectroscopic study at room temperature. The results are illustrated in Figure 4. After excitation at 532 nm, due to high fluorescence, the Raman spectrum of 9AA-HCl does not illustrate any peak in the wave number range of 300–600 cm^{-1}. On the other hand, from the space group theory, it is well known that $A_1 + 2E_2 + E_1$ are the Raman active vibrational modes of the ZnO structure. It is evident from the figure that the Raman spectrum of ZnO NP exhibits four vibration peaks at 328 cm^{-1}, 378 cm^{-1}, 438 cm^{-1} and 577 cm^{-1}, which signifies the presence of a wurtzite structure (Zhang *et al*., 2003). The strong characteristic peak at 438 cm^{-1}can be consigned to the nonpolar optical phonon E_2 mode of ZnO NP at high frequency, which is associated with oxygen deficiency, whereas the peaks at 378 cm^{-1} and 577 cm^{-1} correspond to the polar transverse A_1 and longitudinal E_1 optical phonon modes, respectively. The peak at 332 cm^{-1} is attributed to the E_2^{high}-E_2^{low} mode. The most important thing is that the E_2 mode characteristic band, which is linked to flaws in ZnO NP, changes a lot after conjugation. This change implies that the passivation of the NPs surface states upon binding with the drug molecule. However, the presence of other characteristic bands indicates good wurtzite structure retention during interaction.

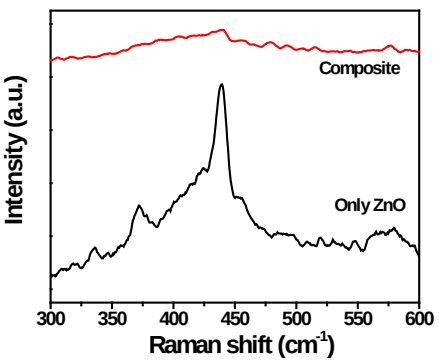

Figure 4: Raman spectra of ZnO NP (black) and conjugates (Red)
(Source: Mitra et al., 2018)

Steady state and Time resolved spectroscopic studies of ZnO-9AA-HCl system

Furthermore, visible spectroscopy helps characterize the nanoconjugate's creation. This therapeutic drug, having two pK_a values (-2.0 and 10.0), can exist in three different forms (Schuldiner *et al*., 1972). In concentrated strong acid (at pH < -2.0), the dominant form of the photodynamic drug is the doubly protonated form, while having -2.0 < pH < 10.0, the protonated form, *i.e.,* 9AAH+, exists. In pH > 10.0, the neutral form prevails through the deprotonation of the protonated form (II) and maintains equilibrium among its amino acids and iminotautomers (Murza *et al*., 2000). Figure 5 displays the UV-vis absorption spectra of only nanoparticles, drug molecules, and the conjugated form, ZnO-9AA-HCl.

At 345 nm, the ZnO NPs show evidence of a threshold band gap of 3.59 eV. However, the drug molecule has the highest absorbance at 400 nm. Note that the spectra of the nanoconjugate show no discernible peak of the drug molecule. The reason for this spectral nature is due to the extremely low concentration of 9AA-HCl and the significant scattering of the ZnO NPs. Moreover, the conjugate's UV-vis peak exhibits a slight shift towards the blue region, compared to the nanoparticle's 338 nm (3.67 eV). Therefore, it is reasonable to conclude that nanohybrids are formed more willingly than only physical absorption due to the interaction between the drug's NP and amine moiety.

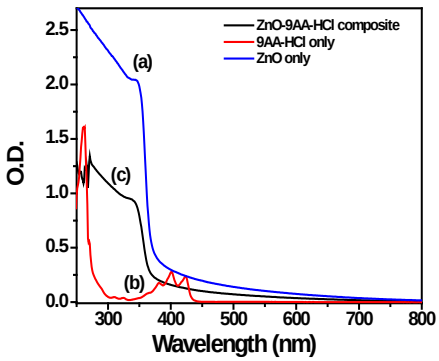

Figure 5: a) ZnO NP, b) 9AA-HCl, and c) ZnO-9AA-HCl; UV-Vis absorption spectra of only nanoparticles *(Source: Mitra et al., 2018)*

The Literature Survey revealed an excited state interaction between NP and carbon dot (Barman *et al*., 2017). Researchers using emission quenching and laser flash photolysis found that light can move electrons between NPs of different sizes and methyl viologen (Mitra *et al*., 2017). NPs, known for their oxygen vacancies, give rise to green emission in the visible region (Vietmeyer *et al*., 2007).

Figure 6(A) portrays suv-visible emission of NP, which is responsible for the surface states. The drug's presence tailors the surface of NPs, eliminating the possibility of energy transfer due to the lack of specific spectral overlap between NPs and drugs. Therefore, in the visible region, the emission quenching is exclusively due to photo-induced electron transfer.

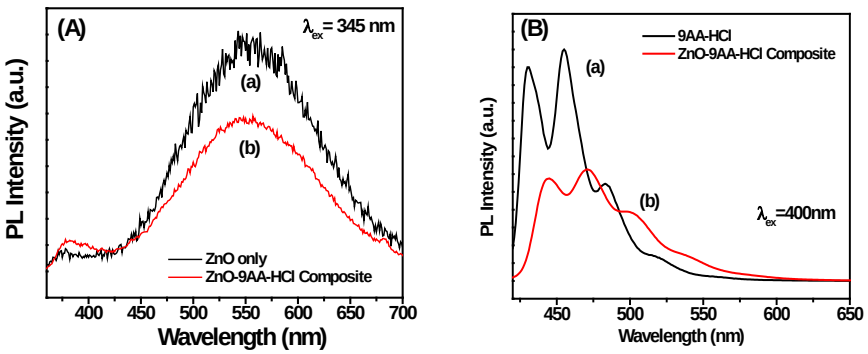

Figure 6: (A) PL spectra (a) NPs and (b) nanoconjugate; (B) PL spectra (a) NPs and (b) nanoconjugate *(Source : Mitra et al., 2018)*

Figure 6 (B) demonstrates the fact that the emission of drug molecules is quenched as well as blue-shifted due to their attachment to NP. Upon conjugation with ZnO NP, the drug molecule's PL spectrum nearly blends into its neutral form. This result indicates that the neutral form of the drug molecule prevails, which might be due to donating the H^+ to the ZnO NP (through hydrogen bonding) after binding with ZnO NP. These modes of binding are well corroborated with the results obtained from FTIR studies, as pointed out in the previous segment.

In order to confirm the occurrence of electron transfer interactions between NP and drug molecules, a time-resolved fluorescence spectroscopic study was performed. To conduct the experiment for the lifetime measurements, 9AA-HCl was excited at a wavelength of 371 nm, and the respective emission was monitored at 455 nm. Pant *et al*. (1986) previously reported the nearly equal lifetimes of the singly protonated and neutral forms. As a result, lifetime measurements are unlikely to identify the species that will prevail during the interaction. There is a single exponential decay in the drug molecule's fluorescence that lasts for 12.89 ns (Figure 7); however, there is a bi-exponential decay in the bioconjugate. The presence of a faster component (0.65 ns with a contribution of 78%) and a slower component (12.87 ns with a contribution of 22%) signify the curve's bi-exponential nature. The slower component, *i.e.,* 12.87 ns, is reliable with the excited-state lifetime of the drug molecule. However, the faster component may be due to the electron migration time from the drug molecule to the NP, as suggested by Kathiravan *et al*. (2009). In this way, the drug molecule adds a second pathway, specifically by connecting 9AA-HCl to ZnO NPs electronically. In addition, the decrease in average lifetime (from 12.89 ns to 3.34 ns) may be linked to the photoinduced electron transfer (PET) from the lowest unoccupied molecular orbital (LUMO) of the drug molecule to the conduction band of the semiconductor through a nonradiative pathway. The apparent non-radiative rate constant (k_{nr}) is determined by

comparing the lifetimes of 9AA-HCl in the absence (τ_0) and in the presence (τ) of ZnO NP, using the following equation:

$$k_{nr} = \frac{1}{<\tau>} - \frac{1}{<\tau_0>} \quad (1)$$

The rate of the electron transfer process from the excited state of the drug molecule to the conduction band of the ZnO NP is estimated to be 1.54×10^9 s^{-1} when considering only the faster component. The obtained k_{nr} value may indicate that the electron transfer process is an ultrafast phenomenon, and it is quite similar to the values reported in the literature (Kathiravan *et al*., 2009). So, having ZnO NPs around could help the PET between the excited state of 9AA-HCl and the semiconductor surface, which would make the photocatalytic and biological actions better.

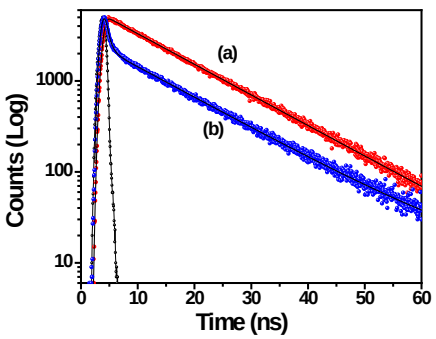

Figure 7: TCSPC curves of (a) the drug molecule and (b) the conjugates Ex-371 nm and Em-455 nm *(Source: Mitra et al., 2018)*

Table 1: *Time-resolved decay parameters of only the drug and the composite, measured at 455 nm under a 371 nm excitation wavelength*

System	τ_1 (ns) [b] (a_1)	τ_2 (ns) [b] (a_2)	τ_{avg} (ns) [b]
9AA-HCl	12.89 (100)	-	12.89
ZnO NP-9AA-HCl	12.87 (0.22)	0.65 (0.78)	3.34

Source: Mitra et al. (2018)

Several experiments have mimicked a natural light harvesting scheme using self-assembled molecules, specifically DNA-conjugated systems and supra-molecular organization of conjugated molecules (fluorophores, dendrimers, organogels, etc.). Adding a fluorophore to a confined matrix is another way to make a light-harvesting device. This gives the molecular arrangement more stability, functionality, and freedom from clumping together. However, the fabrication of light harvesting devices using both donor-acceptor-incorporated host materials encounters several limitations. Firstly, aggregation-based emission quenching may be possible inside the microchannel.

Secondly, it is sometimes necessary for both the donor and acceptor molecules to have similar molecular structures. To avoid such inconveniences, a distinct arrangement of donor-acceptor moieties can be plausible. For this purpose, dye-doped organic-polymer fluorescent nanoparticles may be appropriate as an acceptor system. Furthermore, in the search for a light-absorbing substance, it is currently well established that inorganic nanocrystals, or quantum dots (QDs), are extremely valuable for enhancing the light harvesting process due to their ability to absorb light over a broad spectral window. Particularly, the efficient absorption of visible light by variable-sized quantum dots with tunable band gap energies has established considerable concentration for resourceful solar light energy harvesting systems. To the best of our knowledge, we have not thoroughly studied the rotational relaxation of photoactive molecules inside the polymer nanoparticle, despite it being a suitable means of probing the microenvironment of these nanoparticles. A time-resolved anisotropy study is critical to understanding the source of the dye's rotational relaxation activities inside the polymer nanosphere. The encapsulation of the dye in polymer nanoparticles will constrain its rotational motion. Reorientation times, coupled to the wobbling motion and lateral diffusion of the dye in the nanoparticles, adequately explain the anisotropy decay of the dye molecule in the polymer nanoparticles.

Conclusion

Nowadays, the designing of artificial light harvesting systems using nanomaterials is a challenging task. A thorough understanding of photo physical properties and the carrier relaxation dynamics of photo excited nanocrystals (NCs) is of key importance for both basic research and technological applications. The photo physical properties of semiconductor NCs are considerably different from those of bulk materials as of quantum confinement effect and an enhanced surface-to-volume ratio. The meticulous understanding of the carrier relaxation dynamics is necessary for the reason that it dictates the general efficiency in diverse optoelectronics, photovoltaic, photo catalysis, light-harvesting as well as sensing applications.

Acknowledgement

The author expresses sincere thanks and deep respect to Prof. Amitava Patra. The author extends profound gratitude to Prof. Samita Basu, the research supervisor, for her unwavering cooperation. Special thanks are given to Prof. Nikhil Guchhait for his kind suggestions and discussions whenever needed. The author is deeply indebted to all his colleagues in the Chemistry Department at Triveni Devi Bhalotia College, India for their inspiration. This work would not have been possible without their constant encouragement and support.

References

Abdelmonem, A. M., Pelaz, B., Kantner, K., Bigall, N. C., Del Pino, P., & Parak, W. J. (2015). Charge and agglomeration dependent in vitro uptake and cytotoxicity of zinc oxide nanoparticles. *Journal of Inorganic Biochemistry*, *153*, 334-338. https://doi.org/10.1016/j.jinorgbio.2015.08.029

Barman, M. K., Mitra, P., Bera, R., Das, S., Pramanik, A., & Parta, A. (2017). An efficient charge separation and photocurrent generation in the carbon dot–zinc oxide nanoparticle composite. *Nanoscale*, *9*(20), 6791-6799. https://doi.org/10.1039/C7NR01663H

Cerón-Carrasco, J. P., Ruiz, J., Vicente, C., de Haro, C., Bautista, D., Zuniga, J., & Requena, A. (2017). DFT Simulation of structural and optical properties of 9-aminoacridine half-sandwich Ru (II), Rh (III), and Ir (III) antitumoral complexes and their interaction with DNA. *Journal of Chemical Theory and Computation*, *13*(8), 3898-3910. https://doi.org/10.1021/acs.jctc.7b00139

Cho, N. H., Cheong, T. C., Min, J. H., Wu, J. H., Lee, S. J., Kim, D., ... & Seong, S. Y. (2011). A multifunctional core–shell nanoparticle for dendritic cell-based cancer immunotherapy. *Nature nanotechnology*, *6*(10), 675-682. https://www.nature.com/articles/nnano.2011.149

Das, S., Pramanik, S., Chatterjee, S., Das, P. P., Devi, P. S., & Suresh Kumar, G. (2017). Selective binding of genomic Escherichia coli DNA with ZnO leads to white light emission: a new aspect of nano–bio interaction and interface. *ACS Applied Materials & Interfaces*, *9*(1), 644-657. https://doi.org/10.1021/acsami.6b11109

Graham, L. A., Wilson, G. M., West, T. K., Day, C. S., Kucera, G. L., & Bierbach, U. (2011). Unusual reactivity of a potent platinum–acridine hybrid antitumor agent. *ACS medicinal chemistry letters*, *2*(9), 687-691. https://doi.org/10.1021/ml200104h

He, W., Kim, H. K., Wamer, W. G., Melka, D., Callahan, J. H., & Yin, J. J. (2014). Photogenerated charge carriers and reactive oxygen species in ZnO/Au hybrid nanostructures with enhanced photocatalytic and antibacterial activity. *Journal of the American Chemical Society*, *136*(2), 750-757. https://doi.org/10.1021/ja410800y

Hoffmann, M. R., Martin, S. T., Choi, W., & Bahnemann, D. W. (1995). Environmental applications of semiconductor photocatalysis. *Chemical reviews*, *95*(1), 69-96. https://doi.org/10.1021/cr00033a004

Hu, J., Zhong, Z., Zhang, F., Xing, W., Jin, W., & Xu, N. (2016). High-efficiency, synergistic ZnO-coated SiC photocatalytic filter with antibacterial properties. *Industrial & Engineering Chemistry Research*, *55*(23), 6661-6670. https://doi.org/10.1021/acs.iecr.6b00988

Kathiravan, A., Kumar, P. S., Renganathan, R., & Anandan, S. (2009). Photoinduced electron transfer reactions between meso-tetrakis (4-sulfonatophenyl) porphyrin and colloidal metal-semiconductor nanoparticles. *Colloids and Surfaces A: Physicochemical and Engineering Aspects*, *333*(1-3), 175-181. https://doi.org/10.1016/j.colsurfa.2008.09.042

Kumar, R., Anandan, S., Hembram, K., & Narasinga Rao, T. (2014). Efficient ZnO-based visible-light-driven photocatalyst for antibacterial applications. *Acs applied materials & interfaces*, *6*(15), 13138-13148. https://doi.org/10.1021/am502915v

Latterini, L., & Tarpani, L. (2011). Hierarchical assembly of nanostructures to decouple fluorescence and photothermal effect. *The Journal of Physical Chemistry C*, *115*(43), 21098-21104. https://doi.org/10.1021/jp208124x

Liu, D., Lv, Y., Zhang, M., Liu, Y., Zhu, Y., Zong, R., & Zhu, Y. (2014). Defect-related photoluminescence and photocatalytic properties of porous ZnO nanosheets. *Journal of Materials Chemistry A*, *2*(37), 15377-15388. https://doi.org/10.1039/C4TA02678K

Liu, J., Ma, X., Jin, S., Xue, X., Zhang, C., Wei, T., ... & Liang, X. J. (2016). Zinc oxide nanoparticles as adjuvant to facilitate doxorubicin intracellular accumulation and visualize pH-responsive release for overcoming drug resistance. *Molecular pharmaceutics*, *13*(5), 1723-1730. https://doi.org/10.1021/acs.molpharmaceut.6b00311

Luo, Q. P., Yu, X. Y., Lei, B. X., Chen, H. Y., Kuang, D. B., & Su, C. Y. (2012). Reduced graphene oxide-hierarchical ZnO hollow sphere composites with enhanced photocurrent and photocatalytic activity. *The Journal of Physical Chemistry C*, *116*(14), 8111-8117. https://doi.org/10.1021/jp2113329

Mao, C., Xiang, Y., Liu, X., Cui, Z., Yang, X., Yeung, K. W. K., ... & Wu, S. (2017). Photo-inspired antibacterial activity and wound healing acceleration by hydrogel embedded with Ag/Ag@ AgCl/ZnO nanostructures. *ACS nano*, *11*(9), 9010-9021. https://doi.org/10.1021/acsnano.7b03513

Mitra, P., Dutta, D., Das, S., Basu, T., Pramanik, A., & Patra, A. (2018). Antibacterial and photocatalytic properties of ZnO–9-aminoacridine hydrochloride hydrate drug nanoconjugates. *ACS Omega*, *3*(7), 7962-7970. https://doi.org/10.1021/acsomega.8b00568

Mitra, P., Barman, M. K., Basu, S., Das, S., Pramanik, A., & Patra, A. (2017). Interfacial charge transfer between zinc oxide nanoparticles and methyl viologen: influence of size. *ChemistrySelect*, *2*(30), 9869-9877. https://doi.org/10.1002/slct.201701938

Mitra, P., Chakraborty, P. K., Saha, P., Ray, P., & Basu, S. (2014). Antibacterial efficacy of acridine derivatives conjugated with gold nanoparticles. *International journal of pharmaceutics*, *473*(1-2), 636-643. https://doi.org/10.1016/j.ijpharm.2014.07.051

Mitra, P., Chakraborty, B., & Basu, S. (2014). A spectroscopic investigation of the photophysical behaviour of 9-aminoacridine hydrochloride hydrate in presence of organic amines in homogeneous and heterogeneous media. *Journal of luminescence*, *149*, 221-230. https://doi.org/10.1016/j.jlumin.2014.01.034

Murza, A., Sánchez-Cortés, S., García-Ramos, J. V., Guisan, J. M., Alfonso, C., & Rivas, G. (2000). Interaction of the antitumor drug 9-aminoacridine with guanidinobenzoatase studied by spectroscopic methods: A possible tumor marker probe based on the fluorescence exciplex emission. *Biochemistry*, *39*(34), 10557-10565. https://doi.org/10.1021/bi000583p

Pant, D. D., Joshi, G. C., & Tripathi, H. B. (1986). Photophysics of 9-aminoacridinium hydrochloride. *Pramana*, *27*, 161-170. https://doi.org/10.1007/BF02846336

Rehn, C., & Pindur, U. (1996). Molecular Modeling von Interkalationskomplexen antitumoraktiver 9-Aminoacridine sowie eines [d, e]-anellierten Isochinolinderivates mit basengepaarten Desoxytetranukleotiden. *Monatshefte für Chemie/Chemical Monthly*, *127*, 645-658. https://doi.org/10.1007/BF0081725

Sardar, S., Chaudhuri, S., Kar, P., Sarkar, S., Lemmens, P., & Pal, S. K. (2015). Direct observation of key photoinduced dynamics in a potential nano-delivery vehicle of cancer drugs. *Physical Chemistry Chemical Physics*, *17*(1), 166-177. https://doi.org/10.1039/C4CP03749A

Schuldiner, S., Rottenberg, H., & Avron, M. (1972). Determination of ΔpH in chloroplasts: 2. Fluorescent amines as a probe for the determination of ΔpH in chloroplasts. *European Journal of Biochemistry*, *25*(1), 64-70. https://doi.org/10.1111/j.1432-1033.1972.tb01667.x

Tu, W., Lei, J., Wang, P., & Ju, H. (2011). Photoelectrochemistry of Free-Base-Porphyrin-Functionalized Zinc Oxide Nanoparticles and Their Applications in Biosensing. *Chemistry–A European Journal*, *17*(34), 9440-9447. https://doi.org/10.1002/chem.201100577

Vietmeyer, F., Seger, B., & Kamat, P. V. (2007). Anchoring ZnO particles on functionalized single wall carbon nanotubes. Excited state interactions and charge collection. *Advanced Materials*, *19*(19), 2935-2940. https://doi.org/10.1002/adma.200602773

Mitra, P., Barman, M. K., Basu, S., Das, S., Pramanik, A., & Patra, A. (2017). Interfacial charge transfer between zinc oxide nanoparticles and methyl viologen: influence of size. *ChemistrySelect*, *2*(30), 9869-9877. https://doi.org/10.1002/slct.201701938

Wynn, J. E., Zhang, W., Falkinham III, J. O., & Santos, W. L. (2017). Branched peptides: Acridine and boronic acid derivatives as antimicrobial agents. *ACS medicinal chemistry letters*, *8*(8), 820-823. https://doi.org/10.1021/acsmedchemlett.7b00119

Xiong, H. M. (2013). ZnO nanoparticles applied to bioimaging and drug delivery. *Advanced Materials*, *25*(37), 5329-5335. https://doi.org/10.1002/adma.201301732

Wang, Y. W., Cao, A., Jiang, Y., Zhang, X., Liu, J. H., Liu, Y., & Wang, H. (2014). Superior antibacterial activity of zinc oxide/graphene oxide composites originating from high zinc concentration localized around bacteria. *ACS applied materials & interfaces*, *6*(4), 2791-2798. https://doi.org/10.1021/am4053317

Yuan, Q., Hein, S., & Misra, R. D. K. (2010). New generation of chitosan-encapsulated ZnO quantum dots loaded with drug: synthesis, characterization and in vitro drug delivery response. *Acta biomaterialia*, *6*(7), 2732-2739. https://doi.org/10.1016/j.actbio.2010.01.025

Zhang, J., Zhao, B., Pan, Z., Gu, M., & Punnoose, A. (2015). Synthesis of ZnO nanoparticles with controlled shapes, sizes, aggregations, and surface complex compounds for tuning or switching the photoluminescence. *Crystal Growth & Design*, *15*(7), 3144-3149. https://doi.org/10.1021/cg5017017

Zhang, Y., Jia, H., Wang, R., Chen, C., Luo, X., Yu, D., & Lee, C. (2003). Low-temperature growth and Raman scattering study of vertically aligned ZnO nanowires on Si substrate. *Applied physics letters*, *83*(22), 4631-4633. https://doi.org/10.1063/1.1630849

Zhang, Z. Y., Xu, Y. D., Ma, Y. Y., Qiu, L. L., Wang, Y., Kong, J. L., & Xiong, H. M. (2013). Biodegradable ZnO@ polymer core–shell nanocarriers: pH-triggered release of doxorubicin in vitro. *Angewandte chemie*, *125*(15), 4221-4225. https://doi.org/10.1002/anie.201300431

Zhou, J., Xu, N. S., & Wang, Z. L. (2006). Dissolving behavior and stability of ZnO wires in biofluids: a study on biodegradability and biocompatibility of ZnO nanostructures. *Advanced Materials*, *18*(18), 2432-2435. https://doi.org/10.1002/adma.200600200

Zhou, K., Zhu, Y., Yang, X., Jiang, X., & Li, C. (2011). Preparation of graphene–TiO 2 composites with enhanced photocatalytic activity. *New Journal of Chemistry*, *35*(2), 353-359. https://doi.org/10.1039/C0NJ00623H

Zhu, H., Clark, S. M., Benson, S. C., Rye, H. S., Glazer, A. N., & Mathies, R. A. (1994). High-sensitivity capillary electrophoresis of double-stranded DNA fragments using monomeric and dimeric fluorescent intercalating dyes. *Analytical chemistry*, *66*(13), 1941-1948. https://doi.org/10.1021/ac00085a004